

# Two-component droplet phases and their stability in one dimension

E. G. Charalampidis<sup>1,2,\*</sup> and S. I. Mistakidis<sup>3,†</sup>

<sup>1</sup>*Mathematics Department, California Polytechnic State University, San Luis Obispo, CA 93407-0403, USA*

<sup>2</sup>*Department of Mathematics and Statistics and Computational Science Research Center,  
San Diego State University, San Diego, CA 92182-7720, USA*

<sup>3</sup>*Department of Physics, Missouri University of Science and Technology, Rolla, MO 65409, USA*

(Dated: October 1, 2024)

We unravel the existence and stability properties of one-dimensional droplets arising in genuine two-component particle imbalanced bosonic mixtures under the influence of a weak harmonic confinement. A plethora of miscible droplet phases is found with the majority component atoms in the vicinity of the minority ones assembling in a droplet configuration while the remaining excess atoms being in the gas state. A transition from a bound to a trapped gas many-body state is identified for increasing total atom number and fixed interactions, with the bound character being prolonged for stronger intercomponent attractions. Spectral stability of these two-component droplets is revealed by examining their underlying Bogoliubov-de-Gennes excitation spectrum. Furthermore, the collective dynamics associated with the fundamental dipole and breathing modes of the system is monitored by suddenly shifting the trap's center or quenching the trap's frequency, respectively. A back action of the significantly localized minority component is imprinted in the majority cloud. Our findings can be simulated in recent cold-atom experiments, thus setting the stage for probing the complex nonequilibrium dynamics of two-component droplets.

## I. INTRODUCTION

Quantum droplets are ultradilute and incompressible many-body states of matter arising at attractive interparticle interactions in three-dimensions, and are sustained due to the presence of quantum fluctuations [1–4]. They have been experimentally observed with the aid of recent cold atom simulators originally utilizing dipolar Bose gases [5, 6] and afterwards short-range bosonic mixtures [7–11], thus providing access to beyond mean-field phenomena. According to current investigations, the latter may be predominantly modeled with the dimension [12, 13] and effective range [14, 15] dependent first-order Lee-Huang-Yang (LHY) [16] quantum correction term. This contribution can be consistently incorporated into an extended Gross-Pitaevskii (eGPE) [15, 17] framework, suitable for describing not only droplets, but also other bound states such as bubbles [18, 19] and supersolids [20, 21]. Restricting ourselves to short-range bosonic mixtures that we will study herein, a variety of droplet properties have been explored. These refer, for instance, to ground state droplet configurations [22], their excitation spectrum [23–25], their potential inelastic collisions [22, 26], their coexistence with nonlinear excitations [27–29], rotational properties [30–32], and modulation instability events [33, 34] attributed to their attractive nature.

However, the main focus of the aforementioned studies has been placed on the so-called symmetric droplet scenario where the individual components are identical. This happens when their density ratio is proportional to their intracomponent coupling one resulting in single

droplet yet energetically stable structures [15]. Hence, the actual two-component droplet states are far less explored. In this context, intercomponent atom imbalance is anticipated to result in i) energetically lower and less stable droplets as compared to the symmetric case, and ii) allow the formation of mixed configurations where, depending on the interactions, a portion of the majority component atoms cannot bind to the droplet anymore [35, 36]. Recent investigations explored, to some extent, relevant ground states of droplets in three dimensions (3D), revealing the coexistence of droplet and gas phases, analyzed the interplay of the behavior of their collective modes and self evaporation [35, 36].

In contrast, understanding the existence of highly particle imbalanced two-component droplet states in one-dimension (1D) along with their stability properties is still far from complete [37]. Notable examples here, include rotational droplet properties in a ring geometry [38], lattice trapped droplets building upon a super Tonks-Girardeau gas [39], the existence of multipole droplet states [40], and beyond-LHY approaches to explicate the underlying correlation patterns [4, 37]. Along these lines, the interplay of the distinct components remains an important open issue in 1D, holding the premise of giving rise to unexplored ground states such as mixed droplet-gas configurations, while unveiling, among others, their potential miscibility and back action properties [41] both for statics and dynamics. Additionally, it is still intriguing to explore the conditions under which a droplet to trapped gas transition might take place. In another vein, the dynamical response of the anticipated composite configurations being almost unexplored is on its own an intriguing venue to pursue. We make a first step in this direction herein by monitoring the dynamics of certain collective modes.

To examine the aforementioned possibilities we deploy

\* echaralampidis@sdsu.edu

† smystakidis@mst.edu

an 1D two-component bosonic gas characterized by intracomponent repulsion and intercomponent attraction while featuring high population imbalance. Recall that 1D settings are promising for studying droplet formation due to their lower densities [42, 43]. Indeed, the latter act against lossy mechanisms, and thus self-evaporation being a central issue for the long-time observation of these structures in higher-dimensions [7, 44]. We describe both the static properties and dynamical response of the two-component droplet setting subjected to weak harmonic confinement via the appropriate set of coupled eGPEs incorporating the first-order LHY beyond mean-field correction term [17, 33].

We showcase the existence of distinct miscible two-component particle-imbalanced stationary droplet solutions upon varying the total particle number as well as both intra- and inter-component interactions. Composite configurations are identified with the minority component forming flat-top droplets, whilst the majority one hosts a droplet fragment overlapping with the minority one but existing on top of a finite background whose atoms are in the gas phase. Strikingly, the minority component and the droplet fragment of the majority are separated by a sharp “domain-wall” boundary for strong attractions.

These states bear similarities with the ones identified in the respective 3D setting [35, 36], thus further supporting our current findings which besides extending the aforementioned studies to the 1D realm, they also expose the tunability of ensuing configurations. Indeed, we explicate that the fraction of these individual fragments can be tuned through parametric variations of: i) the involved interactions, ii) particle imbalance, and iii) atom number. We demonstrate among others, that stronger attraction facilitates the decrease of the majority’s droplet segment. Controllable transition from bound state droplets (negative chemical potential) to a trapped gas phase (positive chemical potential) is achieved by tuning the atom number and interactions. Particularly, it is found that the interval of existence of bound states is enhanced for increasing number of atoms predominantly for stronger attractions, and to a lesser extent for increasing imbalance.

The aforementioned two-component droplet states that we identify in this work are shown to be spectrally stable over the atom number or interactions, a finding that is central in our present investigations. This is achieved by numerically extracting the underlying excitation spectrum through a Bogoliubov-de-Gennes (BdG) linearization analysis, thus generalizing the stability of both 1D [18, 23] and two-dimensional (2D) [45, 46] symmetric droplet states. The lowest-lying collective modes, i.e., dipole and breathing, of the resultant spectrum are identified and probed utilizing suitable trap quenches. Namely, it is shown that the dipole mode frequency coincides with that of the trap independently of parametric variations whilst the breathing mode frequency decreases slightly for larger atom numbers. The droplet and the ex-

cess atom fragments of the majority component oscillate in-sync, while a density hump builds atop the majority species distribution as a result of the minority species back action.

This work is organized as follows. Section II, introduces the attractively interacting two-component bosonic system utilized to enter the droplet regime, and the ensuing coupled set of eGPEs used to describe the stationary configurations and nonequilibrium dynamics of two-component droplets. In Section III we analyze the characteristics of the stationary two-component droplet configurations along with their stability properties. Section IV explicates the collective breathing and dipole mode dynamics of the two-component droplets after appropriate quenches of their external traps are applied. We summarize and elaborate on future research directions in Section V.

## II. TWO-COMPONENT BOSE DROPLET

We employ an 1D weakly trapped pseudo-spin-1/2 bosonic system, i.e.,  $m_1 = m_2 \equiv m$ , experiencing particle imbalance ( $N_1 \neq N_2$ ) and lying in the droplet regime. The latter is entered in the case of intracomponent repulsion ( $g_1 \neq g_2 > 0$ ) and intercomponent attraction ( $g_{12} < 0$ ) of the involved spin states but also in the presence of quantum fluctuations that facilitate the generation of droplet configurations [1, 4, 17]. The 1D nature of this setting is warranted due to the weakly harmonic confinement that is elongated in the  $x$  direction with frequency  $\Omega = 10^{-3}$ , and to the strong transverse confinement ( $\Omega_{\perp} \gg \Omega$ ) that essentially prevents structure formation in these directions [47, 48]. In a corresponding experiment, our system may be realized through two distinct hyperfine states of  $^{39}\text{K}$  as in the 3D experiments of Refs. [7, 9].

Specifically, 1D two-component quantum droplets in the presence of the first-order LHY quantum correction and a parabolic external potential are described, in the weakly interacting regime, by the following dimensionless coupled eGPEs [33]

$$i \frac{\partial \Psi_1(x, t)}{\partial t} = \left[ -\frac{1}{2} \frac{\partial^2}{\partial x^2} + (P + GP^{-1})|\Psi_1|^2 - (1 - G)|\Psi_2|^2 - \frac{P}{\pi} \sqrt{P|\Psi_1|^2 + P^{-1}|\Psi_2|^2} + V(x) \right] \Psi_1(x, t), \quad (1a)$$

$$i \frac{\partial \Psi_2(x, t)}{\partial t} = \left[ -\frac{1}{2} \frac{\partial^2}{\partial x^2} + (P^{-1} + GP)|\Psi_2|^2 - (1 - G)|\Psi_1|^2 - \frac{1}{P\pi} \sqrt{P^{-1}|\Psi_2|^2 + P|\Psi_1|^2} + V(x) \right] \Psi_2(x, t). \quad (1b)$$

In these expressions,  $\Psi_j(x, t)$  (with  $j = 1, 2$ ) correspond to the 1D wave function of the  $j$ th component, and  $V(x) = \Omega^2 x^2 / 2$  models the external harmonic trap

of strength  $\Omega$ . We remark that an arguably weak trap is used such that the validity of the LHY contribution holding within the local density approximation [15, 17] is ensured. The impact of the external trap on the LHY form remains still an open issue for future research. Moreover,  $G = 2g\delta g/(g_1 + g_2)^2$ ,  $P = \sqrt{g_1/g_2}$  with  $g = \sqrt{g_1 g_2}$  representing the mean average intracomponent repulsion while  $\delta g = g + g_{12}$  is the mean-field balance point [4, 15]. In the following, we measure the length, time and wave function in terms of  $\xi$ ,  $\hbar/(m\xi^2)$ , and  $\frac{\sqrt{g_1 + \sqrt{g_2}}}{\sqrt{\pi\xi(2|\delta g|)^{2/3}}}$ , where  $\xi = \frac{\hbar^2 \pi}{m} \frac{\sqrt{2|\delta g|}}{g(\sqrt{g_1} + \sqrt{g_2})}$  denotes the healing length [23]. It is interesting to note that the above two-component system can be reduced to an effective single-component one where both components behave identical as long as  $g_1 = g_2 \equiv g$ ,  $N_1 = N_2 \equiv N$  and  $\Psi_1 = \Psi_2 \equiv \Psi$  hold. This single droplet reduction has been extensively studied, see, e.g., the reviews [1, 4], and it arguably hosts less complex configurations than the ones presented next.

### III. EXISTENCE AND STABILITY OF PARTICLE IMBALANCED DROPLETS

Below, we explore the existence of stationary two-component droplet configurations for different atom numbers and intercomponent interactions, while mainly keeping fixed the intracomponent couplings. Subsequently, we study the excitation spectrum of these configurations in order to infer their stability properties.

#### A. Two-component droplet distributions

To visualize the emergent two-component droplet configurations we employ the density distributions of each component, namely  $|\Psi_1(x)|^2$  and  $|\Psi_2(x)|^2$ . These are obtained as follows. We identify stationary states of the system of Eqs. (1) by employing the ansatz

$$\Psi_j(x, t) = \psi_j^{(0)}(x)e^{-i\mu_j t}, \quad (2)$$

where  $\psi_j^{(0)}$  and  $\mu_j$  stand for the stationary wave function and the chemical potential of the  $j$ th component, respectively. Substitution of Eq. (2) into Eqs. (1) leads to the

following time-independent eGPE system

$$\mu_1 \psi_1^{(0)} = -\frac{1}{2}\psi_1^{\prime\prime(0)} + \left[ (P + GP^{-1})|\psi_1^{(0)}|^2 - (1 - G)|\psi_2^{(0)}|^2 - \frac{P}{\pi}\sqrt{P|\psi_1^{(0)}|^2 + P^{-1}|\psi_2^{(0)}|^2 + V(x)} \right] \psi_1^{(0)}, \quad (3a)$$

$$\mu_2 \psi_2^{(0)} = -\frac{1}{2}\psi_2^{\prime\prime(0)} + \left[ (P^{-1} + GP)|\psi_2^{(0)}|^2 - (1 - G)|\psi_1^{(0)}|^2 - \frac{1}{P\pi}\sqrt{P^{-1}|\psi_2^{(0)}|^2 + P|\psi_1^{(0)}|^2 + V(x)} \right] \psi_2^{(0)}(x, t). \quad (3b)$$

Then, we solve Eqs. (3a)-(3b) numerically by using Newton's method [49, 50]. Specifically, we pose the above system on an 1D computational grid with half-width  $L$  (here,  $L = 2000$ ), and discretize derivatives with a centered, fourth-order accurate finite difference scheme with resolution  $dx = 0.1$  while zero Dirichlet boundary conditions are imposed at the edges of the grid. Branches of numerically exact droplet solutions are obtained by utilizing the following strategy.

First, the system of Eqs. (3a)-(3b) is reduced to its single-component counterpart [17] by assuming  $\psi_1 = \psi_2 = \psi$ ,  $\mu_1 = \mu_2 = \mu$ , and  $g_1 = g_2 = g$ . Then, the exact 1D droplet solution of [22] is employed, and fed to our nonlinear solvers as an initial guess. Upon tuning the involved interaction coefficients ( $g_1$ ,  $g_2$ ,  $g_{12}$ ) through numerical continuation [51], we reach specific symmetric droplet configurations having  $N_1 = N_2$ . Here, the number of atoms in each component is given by  $N_j = \int_{-L}^L |\psi_j|^2 dx$ . Consecutively, these solutions are used to determine imbalanced ones by considering parametric variations of either the total particle number  $N_t = cN_1 + (1 - c)N_2$  or the imbalance fraction  $c \in [0, 1]$ , again, through continuation [51]. In both cases, the values of the chemical potentials  $\mu_j$  are obtained in the course of the continuation by adding the algebraic equations  $N_j^{\text{target}} - \int_{-L}^L |\psi_j|^2 dx = 0$  to the nonlinear system of Eqs. (3a)-(3b), where  $N_j^{\text{target}}$  is a “target” value for the  $j$ th atom number. In the following, the characteristics of the two-component droplet configurations having fixed trap frequency  $\Omega = 10^{-3}$  for high and small particle imbalances, i.e., ( $N_1 = 80\%N_t$ ,  $N_2 = 20\%N_t$ ) and ( $N_1 = 60\%N_t$ ,  $N_2 = 40\%N_t$ ), respectively, are analyzed.

The density distributions of the two-component droplet setting featuring ( $N_1 = 80\%N_t$ ,  $N_2 = 20\%N_t$ ) imbalance are depicted in Fig. 1 with respect to the total atom number for weak and strong intercomponent attractions. As it can readily seen, the densities of both the majority and the minority components become wider for increasing atom number, and irrespectively of the intercomponent attraction, see also exemplary density profiles in Fig. 2. The configurations remain always miscible

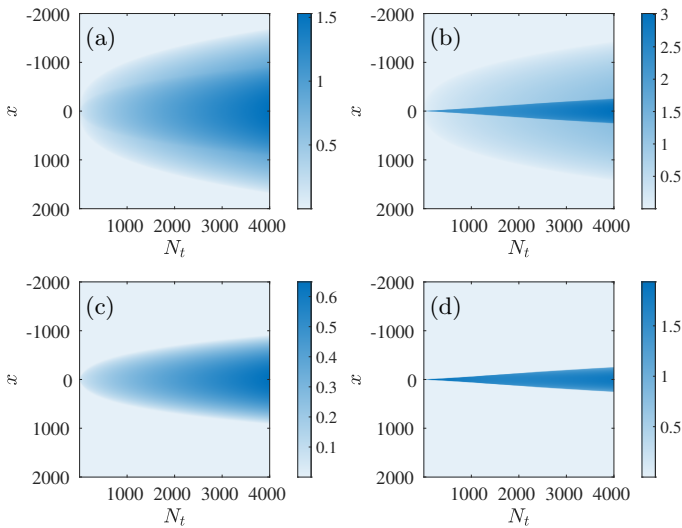


FIG. 1. (Color online) Stationary density distributions of (a), (b) the majority and (c), (d) the minority droplet configurations for  $g_1 = g_2 = 1$ , while (a), (c)  $g_{12} = -0.1$  and (b), (d)  $g_{12} = -0.8$  as a function of the total atom number  $N_t$ . An increasing atom number results in a larger amount of bound majority atoms to the minority ones and a broader distribution of excess particles in the majority. Naturally, this process is more pronounced for stronger intercomponent attractions, see panels (b), (d). The two-component bosonic system features ( $N_1 = 80\%N_t$ ,  $N_2 = 20\%N_t$ ) particle imbalance, and it is subject to a weak harmonic trap of frequency  $\Omega = 10^{-3}$ . All quantities shown are in dimensionless units.

because the minority atoms reside within the majority cloud while binding a portion of the latter in their vicinity. Interestingly, the remaining atoms of the majority component are excess particles, and they do not participate in the droplet part of the mixture. They are rather in a gas state as argued for the corresponding 3D system [35], and contribute negatively to the bound state nature of the total system. This will be shown below by evaluating the involved chemical potentials (see, Fig. 4).

The bound and un-bound portions can be easily discerned in the substantially deformed density distributions especially of the majority component where the central highly localized segment refers to the bound fragment, and the spatially extended tail to the excess atoms as illustrated, for instance, in Figs. 1 and Figs. 2. Such mixed configurations possessing both a droplet portion and excess particles appear to be the energetically lower many-body states of the system, and rise exclusively in the presence of intercomponent imbalance. Indeed, they cannot form in the symmetric droplet case, see, e.g., Refs. [22, 23]. It is also worth noting that the structural deformation of the majority component configurations is reminiscent of anti-dark states, i.e., density humps on top of a finite matter-wave background, which can be generated in repulsive Bose gases [52, 53]. Moreover, this binding mechanism among the majority and the minor-

ity atoms is more pronounced for either fixed interactions and larger atom number, see Figs. 2(d)-(f), or for stronger intercomponent attractions and constant particle imbalance, upon comparing, in particular, Figs. 2(b) and (e).

It is also important to comprehend the explicit gradual deformation of the density distributions of both components for fixed interactions and increasing number of atoms. A “knee” shape pattern starts to appear for relatively small  $N_t$  upon the majority component density around the edges of the minority cloud reflecting the presence of attractive intercomponent interactions. As  $N_t$  increases, these patterns become more prominent, and a larger number of atoms accumulates towards the minority component and bind to it.

This phenomenon can be easily discerned, especially at strong attractions, in the density distributions depicted in Figs. 1(b) and (d), and the profiles illustrated in Fig. 2. Notice also that the minority component tends to form a flat-top configuration, see the insets of Fig. 2(e), (f), manifesting its incompressibility, a characteristic of droplets [15, 54]. The same flat-top signatures occur for the fragment of the majority component distribution which is concentrated around the minority. Moreover, the interface among the minority and the majority distributions is sharp, forming a structure reminiscent of a “domain-wall” which is particularly interesting for dynamical applications of these structures, see Figs. 2(d)-(f). Simultaneously, the fragment of the excess particles grows, and gets manifested by the increasingly extended tails of the majority density distribution. Eventually, we reach a total atom number above which the majority component atoms cannot anymore bind to the droplet segment, and the portion of the excess atoms increases, thus resulting in highly extended density tails. This increasing tendency of the segment of the excess particles is arguably more prominent for stronger intercomponent attractions, e.g., compare Figs. 2(c) and (f).

Signatures of the aforementioned two-component, structurally deformed droplet phases occur also for decreasing particle imbalances until eventually they disappear when the balance limit is approached and the single droplet is attained. An example of low imbalance ( $N_1 = 60\%N$ ,  $N_2 = 40\%N$ ) close to the symmetric system is presented in Fig. 3 for both weak and strong intercomponent attractions. We observe that in the case of weak attractions such as  $g_{12} = -0.1$  [cf. Figs. 1(a) and (c)], both components exhibit a Gaussian-type distribution which becomes wider for larger  $N_t$ . Here, the segment of excess atoms is suppressed and is anticipated to completely vanish for a  $N_1 = N_2 = 50\%N$  mixture. However, an increasing attraction, e.g., to  $g_{12} = -0.8$  enhances the mixed character of the ensuing phases, and in particular, the droplet and gas fragments building upon the majority component become noticeable, see Figs. 3(b) and (d). Of course, they are not comparable to the high particle imbalance setup [cf. Figs. 1(c) and (d)]. Simultaneously, the minority component is signifi-



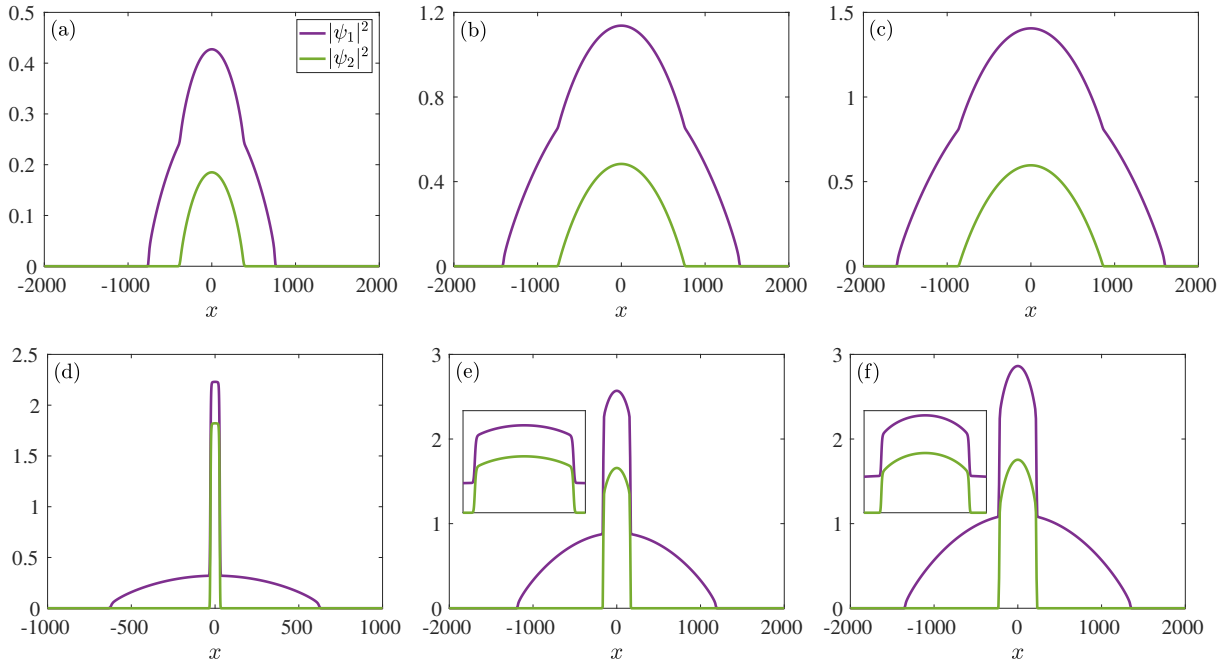


FIG. 2. (Color online) Stationary density profiles of each component (see legends) of the particle imbalanced  $N_1 = 80\%N_t$ ,  $N_2 = 20\%N_t$  bosonic setting for (a), (d)  $N_t = 500$ , (b), (e)  $N_t = 2500$  and (c), (f)  $N_t = 3500$ . The harmonically trapped two-component system with  $\Omega = 10^{-3}$  features  $g_1 = g_2 = 1$  and (a)-(c)  $g_{12} = -0.1$  and (d)-(f)  $g_{12} = -0.8$ . The configurations show a central droplet component and a fraction of excess atoms in the majority component. Insets of panels (e), (f) provide a magnification of the densities at the droplet core showcasing its flat-top shape. The amount of bound atoms of the majority component increases for smaller attractions or larger  $N_t$ . Dimensionless units are utilized for the different parameters.

cantly more localized than the  $g_{12} = -0.1$  case in order to sustain the droplet portion of the many-body state.

### B. Bound state to trapped gas transition

To understand the bound state character of the above-described two-component configurations, we next evaluate not only each of the chemical potentials  $\mu_j$ , but also the total chemical potential,  $\mu_t = \mu_1 + \mu_2$  of the system. Naturally, droplet configurations occur for negative chemical potential, and thus negative energy, since they are self-bound states [2, 3]; otherwise a positive chemical potential implies that a gas state takes place [55]. These chemical potentials are presented in Fig. 4 for different yet fixed interaction configurations ( $g_1, g_2, g_{12}$ ) and varying total atom number,  $N_t$ . We observe that even for small attractions [Figs. 4(a)-(c)] and for relatively small atom numbers ( $N_t < 200$ ),  $\mu_t < 0$ , thus verifying the bound state nature of the entire system. However, its behavior for increasing  $N_t$  depends strongly on both the interactions and the particle imbalance.

Particularly, the chemical potential of the minority component ( $\mu_2$ ) acquires negative values which become larger in magnitude as  $N_t$  increases with the exception of weak attractions and low particle imbalance as is shown

in Fig. 4(c). This trend unveils the bound character of the minority component and thus its droplet nature which is more prominent for either fixed particle imbalance and larger intercomponent attraction, e.g., compare Figs. 4(a) and (d), or fixed interactions and larger imbalance, see for instance Fig. 4(d) and (f). On the other hand, the chemical potential of the majority component,  $\mu_1$ , is positive, and shows a gradual increase for larger  $N_t$ , a behavior that is independent of the interactions or the atom number. This is attributed to the existence of the excess particles in the majority component becoming more prominent as  $N_t$  increases (see, also Fig. 2), and essentially acting against the bound state nature of the ensuing configurations. Hence, the interplay of the chemical potentials of the two components may lead to either a many-body bound state for strong intercomponent attractions as can be seen in Figs. 4(d)-(f), or to a transition of the entire system from a droplet to a trapped gas phase [36] at weaker attractions as  $N_t$  increases, see Figs. 4(a)-(c). Therefore, it is possible to control the bound state character of the many-body system.

It becomes also evident that interactions play a crucial role in the aforementioned transition, i.e., from negative to positive chemical potential. This crossing is shifted to significantly larger atom numbers for stronger intercomponent attractions, see, e.g., Figs. 4(b) and (e). As

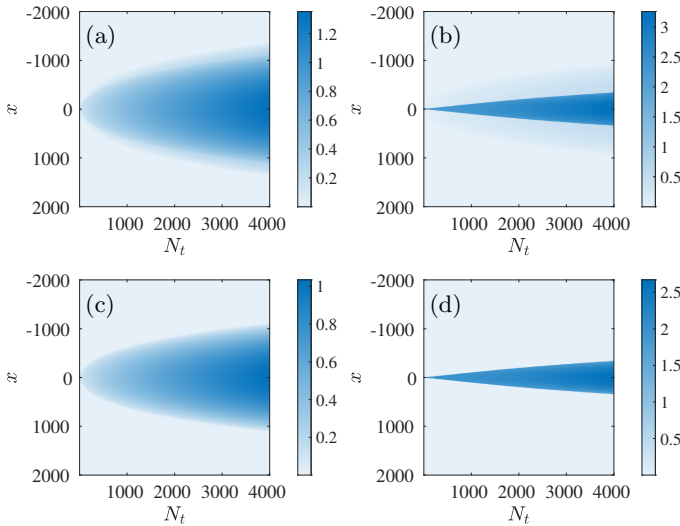


FIG. 3. (Color online) Ground state density distributions for a ( $N_1 = 60\%N$ ,  $N_2 = 40\%N$ ) particle imbalanced system depicting (a), (b) the majority and (c), (d) the minority components in terms of the total atom number  $N_t$ . The respective intracomponent interactions refer to  $g_1 = g_2 = 1$ , and the intercomponent ones are (a), (c)  $g_{12} = -0.1$  and (b), (d)  $g_{12} = -0.8$ . As in the case of ( $N_1 = 80\%N$ ,  $N_2 = 20\%N$ ) presented in Fig. 1 the droplet fragment in the majority component is larger for increasing  $N_t$  at  $g_{12} = -0.8$  [panels (b), (d)]. On the other hand, for smaller attractions, e.g.  $g_{12} = -0.1$  the distribution of each component is Gaussian-type and the segment of excess atoms is suppressed. Other system parameters are the same as in Fig. 1. and are dimensionless.

such, the many-body state cannot maintain its self-bound droplet character throughout the  $N_t$  variation. Additionally, an enhanced intercomponent imbalance such as  $N_1 = 80\%N_t$ ,  $N_2 = 20\%N_t$  sustains the bound character for a wider particle number interval as can be deduced by inspecting Figs. 4(a) and (c). For example, the crossing to positive values occurs at  $N_t \approx 351$  in Fig. 4(a) [ $N_t \approx 280$  in Fig. 4(c)] for a  $N_1 = 80\%N_t$ ,  $N_2 = 20\%N_t$  [ $N_1 = 60\%N_t$ ,  $N_2 = 40\%N_t$ ] imbalance. This can be traced back to the fact that a smaller imbalance is associated with larger total chemical potential, and thus energy of the system, e.g., compare Figs. 4(a) and (c) or Figs. 2(d) and (f). This indeed confirms that strongly particle imbalanced droplets correspond to energetically lower lying configurations. Also, it is worth mentioning that considering intracomponent interaction imbalance while holding fixed all other parameters, a decreasing repulsion accelerates the transition to the gas phase, compare for instance, Figs. 4(d) and (e). Summarizing, the droplet phase is parametrically extended either for fixed particle imbalance and stronger attractions or constant interactions and smaller imbalance, see Fig. 4. We also remark that this transition occurs at smaller  $N_t$  for increasing trap strength (results not shown) since,

in general, the trap does not favor the bound state formation. This was also demonstrated for the respective single-component droplets of a symmetric mixture [56].

### C. Excitation spectrum of particle imbalanced droplets

To infer the spectral stability of the above-described two-component droplet states, we next rely on the so-called BdG analysis [57]. We remark that the excitation spectrum of only 1D symmetric droplet settings has been examined thus far [18, 23] appreciating also the effect of nonlinear excitations [28] and spin-orbit coupling [54]. However, the excitation spectrum of genuine two-component droplet setups that we aim to investigate herein remains highly unexplored.

Specifically, we perturb the obtained stationary solutions,  $\psi_j^{(0)}(x)$  by employing the ansatz

$$\tilde{\psi}_j = e^{-i\mu_j t} \left[ \psi_j^{(0)} + \varepsilon \left( a_j e^{i\omega t} + b_j^* e^{-i\omega^* t} \right) \right], \quad \varepsilon \ll 1. \quad (4)$$

Here, the coefficients  $a_j(x)$  and  $b_j(x)$  denote the corresponding eigenvectors, whilst  $\omega$  are the respective eigenfrequencies. Upon inserting Eq. (4) into Eq. (1), we arrive at order  $\mathcal{O}(\varepsilon)$  at the operator eigenvalue problem

$$-\omega \begin{bmatrix} a_1 \\ b_1 \\ a_2 \\ b_2 \end{bmatrix} = \begin{bmatrix} \mathcal{L}_{11} & \mathcal{L}_{12} & \mathcal{L}_{13} & \mathcal{L}_{14} \\ -\mathcal{L}_{12}^* & -\mathcal{L}_{11} & -\mathcal{L}_{14}^* & -\mathcal{L}_{13}^* \\ \mathcal{L}_{13}^* & \mathcal{L}_{14} & \mathcal{L}_{33} & \mathcal{L}_{34} \\ -\mathcal{L}_{14}^* & -\mathcal{L}_{13} & -\mathcal{L}_{34}^* & -\mathcal{L}_{33} \end{bmatrix} \begin{bmatrix} a_1 \\ b_1 \\ a_2 \\ b_2 \end{bmatrix}, \quad (5)$$

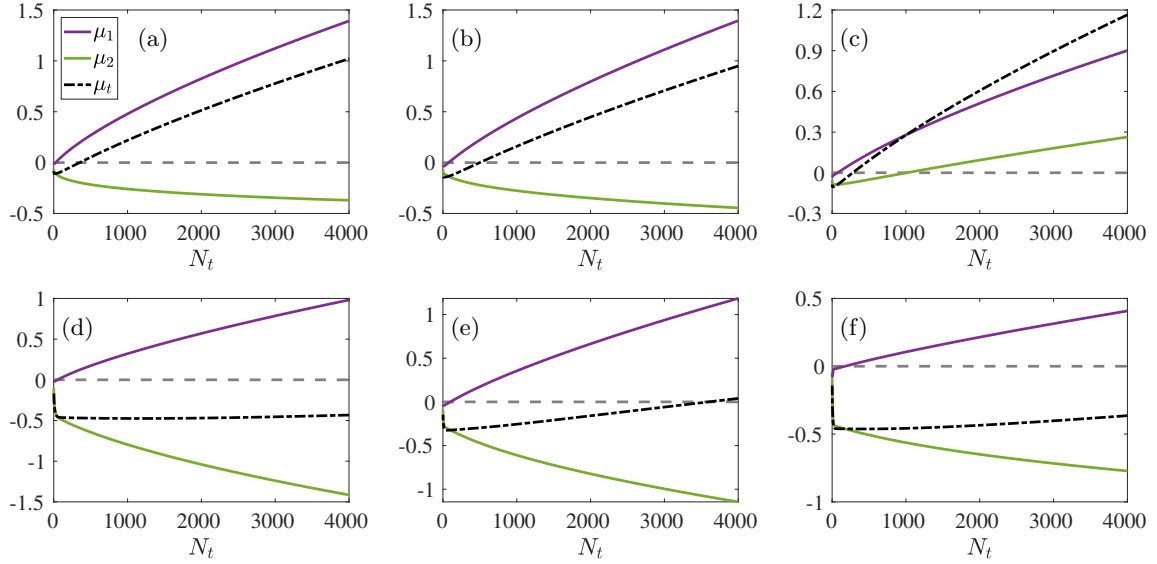


FIG. 4. (Color online) Chemical potential of each component along with the total chemical potential (see the legend in panel (a)) of the particle imbalanced bosonic mixture with respect to the total number of atoms. The two-component droplet setting is characterized by either a  $N_1 = 80\%N_t$  and  $N_2 = 20\%N_t$  [panels (a), (b), (d), and (e)] or a  $N_1 = 60\%N_t$  and  $N_2 = 40\%N_t$  [panels (c) and (f)] imbalance. The ensuing interactions of the different settings correspond to (a), (c)  $g_1 = g_2 = 1$ ,  $g_{12} = -0.1$ , (b)  $g_1 = 1$ ,  $g_2 = 0.5$ ,  $g_{12} = -0.1$ , (d), (f)  $g_1 = g_2 = 1$ ,  $g_{12} = -0.8$  and (e)  $g_1 = 1$ ,  $g_2 = 0.5$ ,  $g_{12} = -0.8$ . The horizontal dashed grey line marks the position of the zero chemical potential. It is evident that at stronger intercomponent attractions (lower panels) the system remains bound having negative total chemical potential. This emanates from the competition among the minority and the majority components featuring negative and positive chemical potentials, respectively. However, a transition from bound to a trapped gas state occurs for smaller attractions, see upper panels. In all cases, an external harmonic trap is present with frequency  $\Omega = 10^{-3}$ , and the depicted quantities are in dimensionless units.

with matrix elements

$$\begin{aligned} \mathcal{L}_{11} = & -\frac{1}{2} \frac{d^2}{dx^2} + 2(P + GP^{-1}) |\psi_1^{(0)}|^2 - (1 - G) |\psi_2^{(0)}|^2 \\ & - \frac{P^2}{2\pi} \frac{|\psi_1^{(0)}|^2}{\sqrt{P|\psi_1^{(0)}|^2 + P^{-1}|\psi_2^{(0)}|^2}} \\ & - \frac{P}{\pi} \sqrt{P|\psi_1^{(0)}|^2 + P^{-1}|\psi_2^{(0)}|^2} + V(x) - \mu_1, \end{aligned} \quad (6a)$$

$$\mathcal{L}_{12} = \left[ (P + GP^{-1}) - \frac{P^2}{2\pi \sqrt{P|\psi_1^{(0)}|^2 + P^{-1}|\psi_2^{(0)}|^2}} \right] (\psi_1^{(0)})^2, \quad (6b)$$

$$\mathcal{L}_{13} = - \left[ (1 - G) + \frac{1}{2\pi \sqrt{P|\psi_1^{(0)}|^2 + P^{-1}|\psi_2^{(0)}|^2}} \right] \psi_1^{(0)} (\psi_2^{(0)})^*, \quad (6c)$$

$$\mathcal{L}_{14} = - \left[ (1 - G) + \frac{1}{2\pi \sqrt{P|\psi_1^{(0)}|^2 + P^{-1}|\psi_2^{(0)}|^2}} \right] \psi_1^{(0)} \psi_2^{(0)}, \quad (6d)$$

$$\begin{aligned} \mathcal{L}_{33} = & -\frac{1}{2} \frac{d^2}{dx^2} + 2(P^{-1} + GP) |\psi_2^{(0)}|^2 - (1 - G) |\psi_1^{(0)}|^2 \\ & - \frac{1}{2P^2\pi} \frac{|\psi_2^{(0)}|^2}{\sqrt{P|\psi_1^{(0)}|^2 + P^{-1}|\psi_2^{(0)}|^2}} \\ & - \frac{1}{P\pi} \sqrt{P|\psi_1^{(0)}|^2 + P^{-1}|\psi_2^{(0)}|^2} + V(x) - \mu_2, \end{aligned} \quad (6e)$$

$$\mathcal{L}_{34} = \left[ (P^{-1} + GP) - \frac{1}{2P^2\pi \sqrt{P|\psi_1^{(0)}|^2 + P^{-1}|\psi_2^{(0)}|^2}} \right] (\psi_2^{(0)})^2. \quad (6f)$$

The solution of the above eigenvalue problem yields the eigenfrequencies  $\omega = \omega_r + i\omega_i$  through which the stability of the pertinent two-component states can be deduced. Recall that a solution is classified as spectrally stable if all the eigenfrequencies  $\omega$  lie on the real axis, i.e., there are no eigenfrequencies with a non-zero imaginary part. On the contrary, if there exist eigenfrequencies with a positive imaginary part, i.e.,  $\omega_i > 0$ , then the solution is deemed unstable. It should be noted that the eigenfrequencies  $\omega$  connect with the eigenvalues  $\lambda$  through a rotation of the spectral plane by  $\pi/2$ , or,  $\omega = i\lambda$ .

The resulting discrete excitation spectra of the highly- and weakly-imbalanced systems referring to ( $N_1 = 80\%N_t$ ,  $N_2 = 20\%N_t$ ) and ( $N_1 = 60\%N_t$ ,  $N_2 = 40\%N_t$ ) respectively are illustrated in Fig. 5 and Fig. 6 as a function of  $N_t$ , and for different intercomponent attractions. Note that we obtain the respective BdG spectra by numerically solving the eigenvalue problem of Eq. (5) for the stationary solutions presented in Figs. 1 and 3. Specifically, Figs. 5 and 6 depict the dependence of the real and imaginary parts of the first eight eigenfrequencies, i.e.,  $\omega_r$  and  $\omega_i$ , respectively, on  $N_t$ . It can be readily deduced that all two-component droplets are spectrally stable, a finding that is supported by the absence of a (positive) imaginary part, i.e.,  $\omega_i = 0$  (being of the order of  $\approx 10^{-7}$  here) in the BdG spectrum, see, panels (b) and (d) of Figs. 5

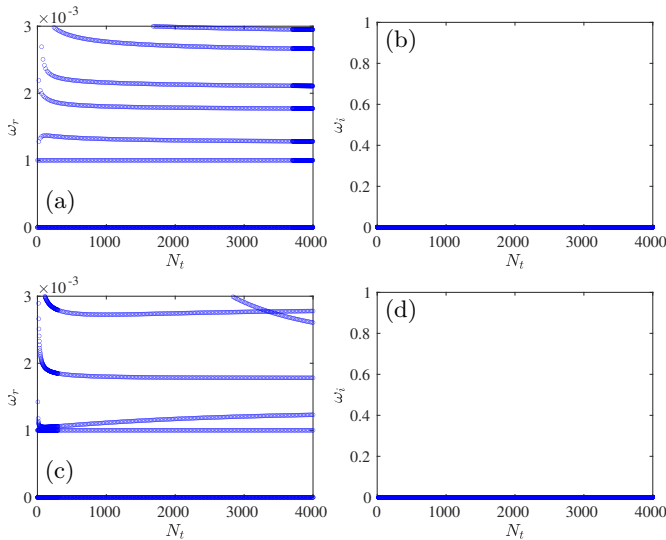


FIG. 5. (Color online) (a), (c) Real and (b), (d) imaginary parts of the BdG excitation spectra for particle imbalanced ( $N_1 = 80\%N_t$ ,  $N_2 = 20\%N_t$ ), droplet configurations upon varying the total atom number  $N_t$ . The scale of the real spectrum being of the order of  $10^{-3}$  reflects the trap frequency  $\Omega = 10^{-3}$ . The two-component settings feature intracomponent repulsion  $g_1 = g_2 = 1$ , and intercomponent attraction (a), (b)  $g_{12} = -0.1$  and (c), (d)  $g_{12} = -0.8$ . Stability of the stationary two-component droplet configurations can be inferred due to the vanishing imaginary part ( $\omega_i = 0$ ) of the spectrum, irrespectively of the atom number and the interactions. All parameters are dimensionless.

and 6. We remark that we have independently verified the validity of our BdG stability results by performing direct dynamical evolution of the above-discussed droplet solutions. The configurations remain intact for times up to  $t = 6000$  that we have checked.

The real part of the BdG spectrum entails information regarding the collective modes of the droplets such as the dipole and the breathing modes appearing at  $\omega_r = \Omega$  and asymptotically at  $\omega_r \approx \sqrt{3}\Omega$ , respectively. These can be traced by monitoring the energetically lowest lying trajectory, and the one around  $\sqrt{3}\Omega$  shown in panels (a) and (c) of Figs. 5 and 6. Here, it is worth pointing out that the values of the collective modes (except of the dipole) depend on  $N_t$ , and hence on the interactions, such as the one of the breathing mode whose thermodynamically predicted value [58, 59] is seen here to be reached for  $N_t > 3000$ . The consistency of our BdG calculations is further supported by the fact that the dipolar mode of frequency  $\omega_r = \Omega (= 10^{-3})$  is persistent in our spectra. From the symmetries point of view, a careful inspection of the spectra reveals the existence of 4 zero, or equivalently, of 2 pairs of zero eigenfrequencies associated with the phase invariance ( $U(1)$  symmetry) of each of the two components. Recall that the space translation invariance is broken due to the presence of the external potential  $V(x)$ , i.e., the eGPE system is no longer translationally

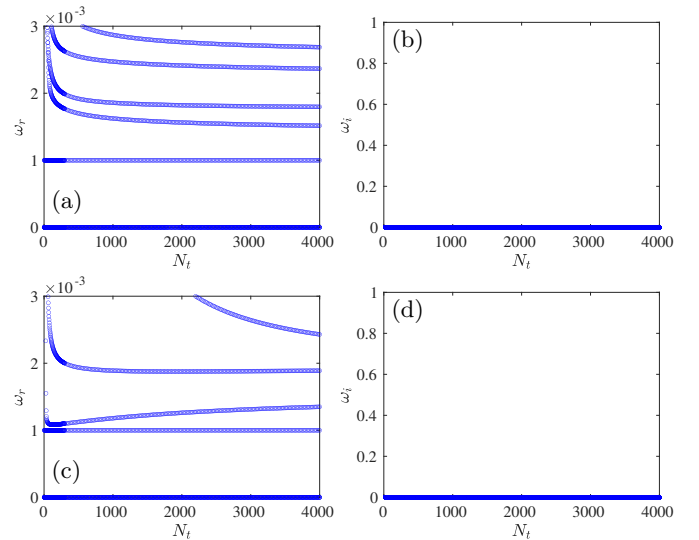


FIG. 6. (Color online) Excitation spectrum of a two-component bosonic droplet system with particle imbalance ( $N_1 = 60\%N_t$ ,  $N_2 = 40\%N_t$ ) with respect to  $N_t$ . Both the (a), (c) real and (b), (d) imaginary parts of  $\omega$  are depicted with  $g_1 = g_2 = 1$ , while (a), (b)  $g_{12} = -0.1$  and (c), (d)  $g_{12} = -0.8$ . Spectral stability of the ensuing two-component droplet states is identified by the absence of imaginary parts in  $\omega$ , i.e.,  $\omega_i = 0$ , for varying atom number and distinct interactions. All quantities are dimensionless.

invariant in  $x$ .

#### IV. COLLECTIVE DYNAMICS OF TWO-COMPONENT DROPLETS

Having analyzed the stationary and stability properties of the particle imbalanced two-component droplet configurations, we subsequently turn our attention to their dynamical behavior. Our aim, here, is in part to verify the predictions of the spectrum regarding some of the appearing mode frequencies, and also visualize basic characteristics of the droplets response that will pave the path for future investigations. As such, the energetically lower fundamental collective modes of the system are studied referring to the droplets dipole and breathing motion. These modes are triggered through appropriate quenches of the external trap, ensuring also that the emergent dynamics can be adequately described by the coupled set of eGPEs. This is because higher-order correlations do not play a significant role as it was argued for symmetric droplets [56, 59]. Namely, a sudden shift of the trap's center results in exciting the dipole motion, while an abrupt change of the trap's frequency induces the breathing dynamics of the components.

Below, we present the time-evolution of representative cases of two-component droplets corresponding to different total atom numbers while maintaining the im-

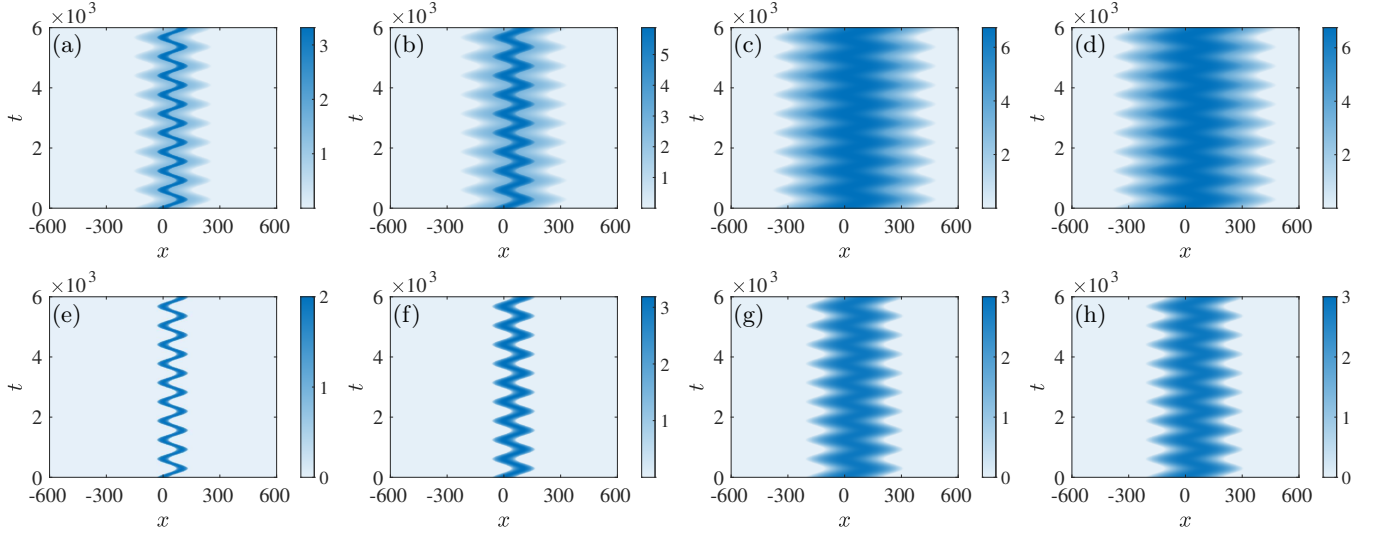


FIG. 7. (Color online) Time evolution of the droplet densities of each component following a sudden change of the trap's center from  $x_0 = 0$  to  $x_0 = +50$ . The intercomponent particle imbalance is fixed to ( $N_1 = 80\%N_t$ ,  $N_2 = 20\%N_t$ ), while the total atom number corresponds to (a), (e)  $N_t = 500$ , (b), (f)  $N_t = 1500$ , (c), (g)  $N_t = 3980$  and (d), (h)  $N_t = 3999$ . Apparently, both the majority (upper panels) and the minority (lower panels) components perform a collective dipole motion reflected by their in-phase oscillation within the trap. In particular, for lower atom numbers where the minority is highly localized imprints its motion to the majority component cloud. In all cases, the two-component bosonic droplet is initiated in its ground state configuration with interactions  $g_1 = g_2 = 1$  and  $g_{12} = -0.8$ , while being under the influence of an external harmonic trap with frequency  $\Omega = 10^{-2}$ . All quantities shown are in dimensionless units.

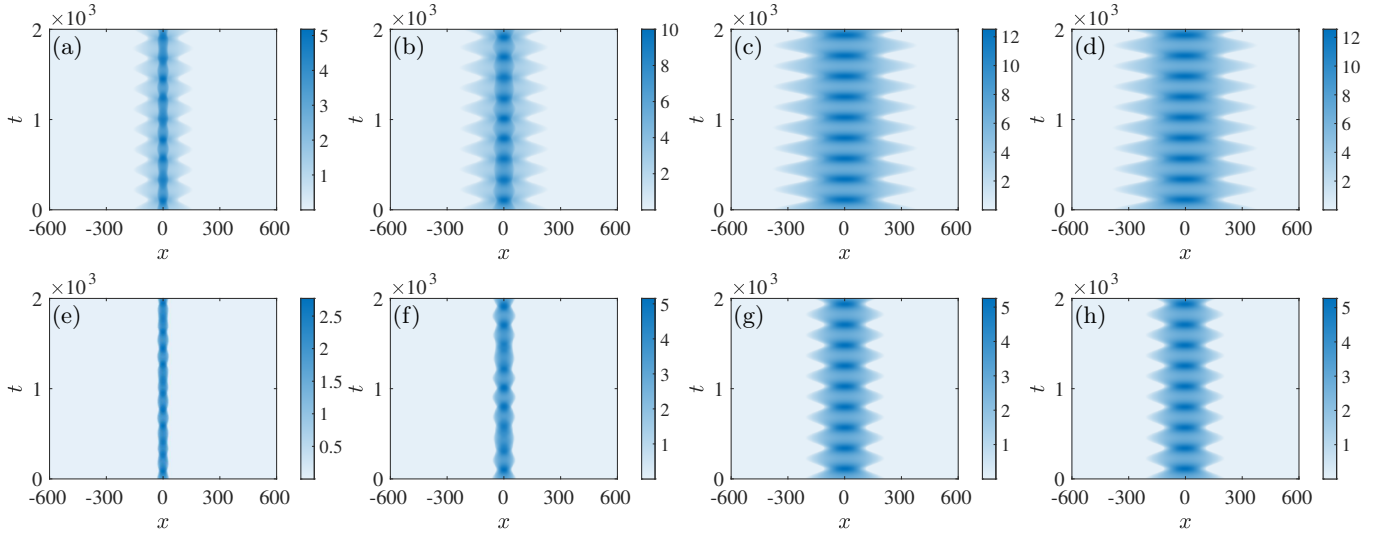


FIG. 8. (Color online) Dynamics of the individual component droplet density distributions after a quench of the trap frequency from  $\Omega = 10^{-2}$  to  $\Omega_f = \pi\Omega/2 \approx 1.6 \times 10^{-2}$ . Different configurations are depicted associated with (a), (e)  $N_t = 500$ , (b), (f)  $N_t = 1500$ , (c), (g)  $N_t = 3980$  and (d), (h)  $N_t = 3999$ . The quench triggers a periodic expansion and contraction dynamics of both the majority (upper panels) and the minority (lower panels) clouds. Both the droplet and excess atom segments of the majority component move in-sync and the backaction of the highly localized minority component to the majority one is evident for smaller atom numbers. The system is prepared in its ground state characterized by ( $N_1 = 80\%N_t$ ,  $N_2 = 20\%N_t$ ),  $g_1 = g_2 = 1$ ,  $g_{12} = -0.8$  and  $\Omega = 10^{-2}$ . Quantities are presented in dimensionless units.

balance ( $N_1 = 80\%N_t$ ,  $N_2 = 20\%N_t$ ) and interactions ( $g_{11} = g_{22} = 1$ ,  $g_{12} = -0.8$ ), see also Fig. 1 and Fig. 2. A similar phenomenology occurs for other intercomponent interactions (not shown for brevity), while as the particle imbalance is decreased and the system tends to acquire equal intercomponent population, we retrieve the known characteristics of the symmetric droplet mixture reported, for instance, in Refs [59, 60]. To better visualize the emergent collective dynamics in somewhat smaller timescales, we use a slightly tighter trap, as compared to the above sections, characterized by  $\Omega = 10^{-2}$ .

The spatiotemporal density dynamics of both components after a quench of each component's trap center from  $x_0 = 0$  to  $x_0 = +50$  for  $N_t = 500$ ,  $N_t = 1500$ ,  $N_t = 3980$  and  $N_t = 3999$  is depicted in Fig. 7. In all cases, both components perform a collective in-trap oscillatory motion with frequency equal to the one of the trap. This is a clear manifestation of the excitation of the dipole mode. Notice that the dipole mode frequency is measured through the spectrum of the time-evolved center-of-mass of each individual cloud. It is found that independently of  $N_t$  or the interactions, and hence the ensuing droplet configurations, the dipole mode frequency is unchanged which further confirms the BdG outcome of Figs. 5(c) and (d), where  $\omega_r = \Omega$ . Interestingly, for smaller  $N_t$ , where the spatial localization of the minority component distribution is more enhanced and the droplet fraction smaller, we observe a prominent back action to the majority component as a consequence of the intercomponent attraction. Here, a density hump builds upon the majority component distribution imprinting the minority's trajectory. In this case, both the droplet and excess atom fragments of the majority component oscillate in-phase, see Figs. 7(a), (b), (e), and (f). This suggests that the droplet fragment of the composite configuration drifts the gaseous one. On the other hand, and for larger  $N_t$  (where the droplet fraction increases), it can be seen that the aforementioned two segments of the majority component are hardly discernible, and the cloud undergoes an overall oscillatory behavior as is shown in Figs. 7(c), (d), (g), and (h).

The breathing mode of the droplet is triggered by quenching the trap's frequency, and corresponds to a collective expansion and contraction of each component distribution in a periodic manner. The time-evolution of the densities of both participating components are illustrated in Figs. 8 for the same atom numbers used for the dipole mode. We estimate the underlying breathing mode frequency by monitoring the dynamics of the width of the individual wavepackets [61, 62], and evaluating its spectrum. We find that the breathing mode frequency exhibits an interaction dependent behavior for both components, and in particular, it features a slightly decreasing tendency for larger  $N_t$  while being eventually saturated for  $N_t > 3000$  to  $\approx \sqrt{3}\Omega$ . Interestingly, the minority component for relatively small  $N_t$ , see Figs. 8(e) and (f), has two distinguishable breathing frequencies one of them coinciding with the breathing frequency of the major-

ity component and the other being slightly larger. This two-mode response of the minority hints towards a few-body effect which becomes suppressed for larger  $N_t$ , see Figs. 8(g), (h).

This overall behavior but also the values of the breathing frequency extracted from the dynamics match the predictions of the BdG spectrum. Furthermore, as in the case of the dipole mode dynamics discussed above, the back action of the spatially localized minority component into the majority one is well discernible for relative small  $N_t$ . This can be readily seen in the density evolution of the majority component presented in Figs. 8(a), (b), (e), and (f) where traces of the minority distribution are evident and manifest themselves as density undulations of the otherwise smooth (flat-top type) droplet core. Once again, both fragments constituting the majority component move in-sync implying that the droplet part governs the dynamical response. However, as  $N_t$  increases, the breathing amplitude becomes more intense and its frequency decreases, compare, for instance, Figs. 8(e) and (g), while the majority component fragments are less distinguishable, see Figs. 7(c), (d), (g), and (h).

## V. SUMMARY AND PERSPECTIVES

We examined the existence and stability of two-component particle imbalanced droplet phases in 1D as captured by the appropriate coupled set of eGPEs taking into account the LHY quantum correction term. In particular, the system under investigation is a particle imbalanced homonuclear two-component bosonic mixture featuring intracomponent repulsion and intercomponent attraction, while being weakly confined by an external harmonic trap. Along with the characteristics of the underlying stationary states, we inspect the droplets' excitation spectrum and also dynamically probe the droplets' fundamental dipole and breathing modes by utilizing suitable quenches of the external trap.

Focusing on the ground state of the system, a multitude of complex droplet states is identified with respect to the atom number for different imbalances and interaction configurations. It is found that the involved components remain miscible in nature for the different parametric variations considered, while hosting highly deformed configurations. Namely, the minority component sustains a flat-top type droplet but the majority species exhibits mixed configurations forming a droplet in the vicinity of the minority and excess atoms reside in a gas state at the tails of the distribution density. These mixed phases appear to be more prominent for either increasing total atom number and stronger intercomponent attractions while keeping the imbalance fixed or in general for larger imbalance fraction. Naturally, larger attractions support stronger binding among the components but lead to a smaller droplet fragment. Along the same lines, a fixed imbalance leads to increasingly spatially extended distributions and favors the formation of larger droplet and



excess atoms segments for increasing atom number.

To infer the bound state character of the ensuing two-component configurations, we evaluate the chemical potential of each component separately and the one of the entire system. It is explicated that the bound character of the system is highly tunable meaning that it may either remain bound or experience a transition to a trapped gas state (mainly depending on the considered interactions or particle imbalance). This is traced back to the interplay of the individual components with the minority one possessing negative chemical potential, and the majority featuring predominantly positive chemical potentials due to the existence of excess atoms. Overall, the parametric regions of bound state formation are extended in terms of the total atom number for stronger attractions or larger imbalances with the former having an arguably more substantial effect. As expected, smaller imbalances are associated with lower-lying composite states. Additionally, by numerically calculating the corresponding eGPEs excitation spectrum via BdG analysis, it is demonstrated that the aforementioned two-component droplet states are spectrally stable over particle imbalance, atom number, and interaction variations. Indeed, the spectrum contains vanishing imaginary parts, whereas its real part connects with the droplets' collective modes that we were able to identify. Recall that this stability outcome is in line with earlier predictions in the symmetric mixture case [18, 23].

To trigger some of the characteristic droplet modes in the dynamics, we employ quenches where in particular a trap shift induces the droplets dipole motion and a change of the trap frequency promotes their breathing evolution. The former manifests as a collective in-trap oscillation of the individual clouds and the latter as a periodic expansion and contraction dynamics of the droplet distributions. In both cases, the measured oscillation frequencies match with the predictions of the excitation spectrum, i.e., the dipole mode frequency is insensitive to atom number variations and the breathing mode one slightly increases for larger atom numbers. Interestingly, for low atom numbers where the minority component is substantially localized, we observe that its

trajectory is imprinted in the majority cloud as a result of back action. In all cases, the droplet and the excess atom fragments of the majority species oscillate in-sync.

Our findings pave the way for various fruitful extensions, aiming to advance our understanding on multicomponent droplet settings. In this context, it would be intriguing to examine the emergent nonequilibrium dynamics of the imbalanced two-component droplet states, such as nucleated patterns and the role of modulation instability [33] by considering, for instance, interaction quenches across the localized to delocalized phases of the minority atoms. Moreover, the generalization of our results in higher dimensions (with the appropriate modification of the LHY term) intending to reveal the interplay of transverse modes on the droplet formation is of immense interest. In that vein, the computational framework developed in [63] together with deflation-based techniques [64–67] will be the principal vehicle for these higher-dimensional studies. Also, the characterization of strongly interacting two-component droplet phases requiring the utilization of beyond eGPE techniques such as the ab-initio ML-MCTDHX method [68] or exact diagonalization [69], for exploring the underlying correlation patterns and excitation processes is certainly desirable. Finally, extending our present considerations to three-component systems, especially for imbalanced mixtures which are expected to host far richer phases and to have more complex stability properties would be worth pursuing. All these are exciting future research directions that are currently under consideration, and results will be reported in forthcoming works.

## ACKNOWLEDGEMENTS

EGC is supported by the U.S. National Science Foundation under Grant No. DMS-2204782. S. I. M acknowledges support from the Missouri Science and Technology, Department of Physics, Startup fund. S. I. M thanks P. G. Kevrekidis, G.C Katsimiga, G. B. Bougas, and J. Pelayo for fruitful discussions.

- 
- [1] Z.-H. Luo, W. Pang, B. Liu, Y.-Y. Li, and B. A. Malomed, *Front. Phys.* **16** (2020), 10.1007/s11467-020-1020-2.
  - [2] F. Böttcher, J.-N. Schmidt, J. Hertkorn, K. S. Ng, S. D. Graham, M. Guo, T. Langen, and T. Pfau, *Rep. Prog. Phys.* **84**, 012403 (2020).
  - [3] L. Chomaz, I. Ferrier-Barbut, F. Ferlaino, B. Laburthe-Tolra, B. L. Lev, and T. Pfau, *Rep. Progr. Phys.* **86**, 026401 (2022).
  - [4] S. I. Mistakidis, A. G. Volosniev, R. E. Barfknecht, T. Fogarty, T. Busch, A. Foerster, P. Schmelcher, and N. T. Zinner, *Phys. Rep.* **1042**, 1 (2023).
  - [5] M. Schmitt, M. Wenzel, F. Böttcher, I. Ferrier-Barbut, and T. Pfau, *Nature* **539**, 259 (2016).
  - [6] L. Chomaz, S. Baier, D. Petter, M. Mark, F. Wächtler, L. Santos, and F. Ferlaino, *Phys. Rev. X* **6**, 041039 (2016).
  - [7] C. R. Cabrera, L. Tanzi, J. Sanz, B. Naylor, P. Thomas, P. Cheiney, and L. Tarruell, *Science* **359**, 301 (2018).
  - [8] P. Cheiney, C. R. Cabrera, J. Sanz, B. Naylor, L. Tanzi, and L. Tarruell, *Phys. Rev. Lett.* **120**, 135301 (2018).
  - [9] G. Semeghini, G. Ferioli, L. Masi, C. Mazzinghi, L. Wolswijk, F. Minardi, M. Modugno, G. Modugno, M. Inguscio, and M. Fattori, *Phys. Rev. Lett.* **120**, 235301 (2018).
  - [10] C. D'Errico, A. Burchianti, M. Prevedelli, L. Salasnich, F. Ancilotto, M. Modugno, F. Minardi, and C. Fort, *Phys. Rev. Res.* **1**, 033155 (2019).



- [11] Z. Guo, F. Jia, L. Li, Y. Ma, J. M. Hutson, X. Cui, and D. Wang, *Phys. Rev. Res.* **3**, 033247 (2021).
- [12] P. Zin, M. Pylak, T. Wasak, M. Gajda, and Z. Idziaszek, *Phys. Rev. A* **98**, 051603 (2018).
- [13] J. C. Pelayo, G. Bougas, T. Fogarty, T. Busch, and S. I. Mistakidis, arXiv:2407.16383 (2024).
- [14] R. Schützhold, M. Uhlmann, Y. Xu, and U. R. Fischer, *Int. J. Mod. Phys. B* **20**, 3555 (2006).
- [15] D. S. Petrov, *Phys. Rev. Lett.* **115**, 155302 (2015).
- [16] I. L.-T. Properties, *Selected Papers (1945-1980) Of Chen Ning Yang (With Commentary)* **36**, 212 (2005).
- [17] D. S. Petrov and G. E. Astrakharchik, *Phys. Rev. Lett.* **117**, 100401 (2016).
- [18] G. C. Katsimiga, S. I. Mistakidis, B. A. Malomed, D. J. Frantzeskakis, R. Carretero-Gonzalez, and P. G. Kevrekidis, *Condens. Matter* **8**, 67 (2023).
- [19] M. Edmonds, *Phys. Rev. Res.* **5**, 023175 (2023).
- [20] P. B. Blakie, D. Baillie, L. Chomaz, and F. Ferlaino, *Phys. Rev. Res.* **2**, 043318 (2020).
- [21] T. Bland, E. Poli, C. Politi, L. Klaus, M. A. Norcia, F. Ferlaino, L. Santos, and R. N. Bisset, *Phys. Rev. Lett.* **128**, 195302 (2022).
- [22] G. E. Astrakharchik and B. A. Malomed, *Phys. Rev. A* **98**, 013631 (2018).
- [23] M. Tylutki, G. E. Astrakharchik, B. A. Malomed, and D. S. Petrov, *Phys. Rev. A* **101**, 051601 (2020).
- [24] H. Hu and X.-J. Liu, *Phys. Rev. A* **102**, 053303 (2020).
- [25] P. Stürmer, M. N. Tengstrand, R. Sachdeva, and S. M. Reimann, *Phys. Rev. A* **103**, 053302 (2021).
- [26] G. Ferioli, G. Semeghini, L. Masi, G. Giusti, G. Modugno, M. Inguscio, A. Galemí, A. Recati, and M. Fattori, *Phys. Rev. Lett.* **122**, 090401 (2019).
- [27] Y. Li, Z. Chen, Z. Luo, C. Huang, H. Tan, W. Pang, and B. A. Malomed, *Phys. Rev. A* **98**, 063602 (2018).
- [28] G. C. Katsimiga, S. I. Mistakidis, G. N. Koutsokostas, D. J. Frantzeskakis, R. Carretero-González, and P. G. Kevrekidis, *Phys. Rev. A* **107**, 063308 (2023).
- [29] Y. V. Kartashov, V. M. Lashkin, M. Modugno, and L. Torner, *New J. Phys.* **24**, 073012 (2022).
- [30] M. N. Tengstrand, P. Stürmer, E. O. Karabulut, and S. M. Reimann, *Phys. Rev. Lett.* **123**, 160405 (2019).
- [31] T. A. Yoğurt, U. Tanyeri, A. Keleş, and M. O. Oktel, *Phys. Rev. A* **108**, 033315 (2023).
- [32] L. Dong and Y. V. Kartashov, *Phys. Rev. Lett.* **126**, 244101 (2021).
- [33] T. Mithun, A. Maluckov, K. Kasamatsu, B. A. Malomed, and A. Khare, *Symmetry* **12**, 174 (2020).
- [34] S. R. Otajonov, E. N. Tsoy, and F. K. Abdullaev, *Phys. Rev. A* **106**, 033309 (2022).
- [35] T. A. Flynn, L. Parisi, T. P. Billam, and N. G. Parker, *Phys. Rev. Res.* **5**, 033167 (2023).
- [36] T. A. Flynn, N. A. Keeper, N. G. Parker, and T. P. Billam, *Phys. Rev. Res.* **6**, 013209 (2024).
- [37] I. A. Englezos, P. Schmelcher, and S. I. Mistakidis, *Phys. Rev. A* **110**, 023324 (2024).
- [38] M. N. Tengstrand and S. M. Reimann, *Phys. Rev. A* **105**, 033319 (2022).
- [39] J. Vallès-Muns, I. Morera, G. E. Astrakharchik, and B. Juliá-Díaz, *SciPost Phys.* **16**, 074 (2024).
- [40] Y. V. Kartashov and D. A. Zezyulin, *Phys. Rev. A* **110**, L021304 (2024).
- [41] J. C. Pelayo, T. Fogarty, T. Busch, and S. I. Mistakidis, *Phys. Rev. Res.* **6**, 033219 (2024).
- [42] L. Lavoine and T. Bourdel, *Phys. Rev. A* **103**, 033312 (2021).
- [43] B. L. Tolra, K. M. O'Hara, J. H. Huckans, W. D. Phillips, S. L. Rolston, and J. V. Porto, *Phys. Rev. Lett.* **92**, 190401 (2004).
- [44] C. Fort and M. Modugno, *Applied Sciences* **11**, 866 (2021).
- [45] Y. Li, Z. Chen, Z. Luo, C. Huang, H. Tan, W. Pang, and B. A. Malomed, *Phys. Rev. A* **98**, 063602 (2018).
- [46] G. Bougas, G. C. Katsimiga, P. G. Kevrekidis, and S. I. Mistakidis, arXiv:2405.20106 (2024).
- [47] A. Görlitz, J. M. Vogels, A. E. Leanhardt, C. Raman, T. L. Gustavson, J. R. Abo-Shaeer, A. P. Chikkatur, S. Gupta, S. Inouye, T. Rosenband, and W. Ketterle, *Phys. Rev. Lett.* **87**, 130402 (2001).
- [48] A. Romero-Ros, G. C. Katsimiga, S. I. Mistakidis, S. Mossman, G. Biondini, P. Schmelcher, P. Engels, and P. G. Kevrekidis, *Phys. Rev. Lett.* **132**, 033402 (2024).
- [49] C. Kelley, *Solving Nonlinear Equations with Newton's Method* (Fundamentals of Algorithms, Society of Industrial and Applied Mathematics (Philadelphia), 2003).
- [50] C. Kelley, *Iterative Methods for Linear and Nonlinear Equations* (Frontiers in Applied Mathematics, Society of Industrial and Applied Mathematics (Philadelphia), 1995).
- [51] Y. Kuznetsov, *Elements of Bifurcation Theory (4th Edition)* (Springer-Verlag (New York), 2023).
- [52] C. Qu, L. P. Pitaevskii, and S. Stringari, *Phys. Rev. Lett.* **116**, 160402 (2016).
- [53] G. C. Katsimiga, S. I. Mistakidis, T. M. Bersano, M. K. H. Ome, S. M. Mossman, K. Mukherjee, P. Schmelcher, P. Engels, and P. G. Kevrekidis, *Phys. Rev. A* **102**, 023301 (2020).
- [54] S. Gangwar, R. Ravisankar, S. I. Mistakidis, P. Muruganandam, and P. K. Mishra, *Phys. Rev. A* **109**, 013321 (2024).
- [55] C. J. Pethick and H. Smith, *Bose-Einstein condensation in dilute gases* (Cambridge university press, 2008).
- [56] S. I. Mistakidis, T. Mithun, P. G. Kevrekidis, H. R. Sadeghpour, and P. Schmelcher, *Phys. Rev. Res.* **3**, 043128 (2021).
- [57] N. N. Bogolyubov, *Izv. Akad. Nauk SSSR, Ser. Fiz.* **11**, 77 (1947).
- [58] J. Abraham and M. Bonitz, *Contributions to Plasma Physics* **54**, 27 (2014).
- [59] I. A. Englezos, S. I. Mistakidis, and P. Schmelcher, *Phys. Rev. A* **107**, 023320 (2023).
- [60] L. Parisi and S. Giorgini, *Phys. Rev. A* **102**, 023318 (2020).
- [61] J. P. Ronzheimer, M. Schreiber, S. Braun, S. S. Hodgman, S. Langer, I. P. McCulloch, F. Heidrich-Meisner, I. Bloch, and U. Schneider, *Phys. Rev. Lett.* **110**, 205301 (2013).
- [62] T. Fukuhara, A. Kantian, M. Endres, M. Cheneau, P. Schauß, S. Hild, D. Bellem, U. Schollwöck, T. Giamarchi, C. Gross, I. Bloch, and S. Kuhr, *Nature Phys.* **9**, 235 (2013).
- [63] G. Sadaka, P. Jolivet, E. G. Charalampidis, and I. Danaila, *Computer Physics Communications* **306**, 109378 (2025).
- [64] E. Charalampidis, P. Kevrekidis, and P. Farrell, *Communications in Nonlinear Science and Numerical Simulation* **54**, 482 (2018).

- [65] N. Boullé, E. G. Charalampidis, P. E. Farrell, and P. G. Kevrekidis, *Phys. Rev. A* **102**, 053307 (2020).
- [66] E. Charalampidis, N. Boullé, P. Farrell, and P. Kevrekidis, *Communications in Nonlinear Science and Numerical Simulation* **87**, 105255 (2020).
- [67] N. Boullé, I. Newell, P. E. Farrell, and P. G. Kevrekidis, *Phys. Rev. A* **107**, 012813 (2023).
- [68] L. Cao, V. Bolsinger, S. I. Mistakidis, G. Koutentakis, S. Krönke, J. Schurer, and P. Schmelcher, *The Journal of chemical physics* **147** (2017).
- [69] L. Chergui, J. Bengtsson, J. Bjerlin, P. Stürmer, G. M. Kavoulakis, and S. M. Reimann, *Phys. Rev. A* **108**, 023313 (2023).